Epithelial Layer Fluidization by Curvature-Induced Unjamming

Margherita De Marzio,[1,2,*] Amit Das,[3] Jeffrey J. Fredberg,[2] and Dapeng Bi[4,†]
[1]Channing Division of Network Medicine, Brigham and Women's Hospital and Harvard Medical School, Boston, Massachusetts 02115, USA
[2]Harvard T. H. Chan School of Public Health, Boston, Massachusetts 02115, USA
[3]Department of Biochemical Engineering and Biotechnology, IIT Delhi, New Delhi, India
[4]Department of Physics and the Center for Theoretical Biological Physics, Northeastern University, Boston, Massachusetts 02115, USA

(Received 21 May 2023; accepted 4 March 2025; published 3 April 2025)

The transition of an epithelial layer from a stationary, quiescent state to a highly migratory, dynamic state is required for wound healing, development, and regeneration. This transition, known as the unjamming transition (UJT), is responsible for epithelial fluidization and collective migration. Previous theoretical models have primarily focused on the UJT in flat epithelial layers, neglecting the effects of strong surface curvature characteristic of the epithelium *in vivo*. In this Letter, we investigate the role of surface curvature on tissue plasticity and cellular migration using a vertex model embedded on a spherical surface. Our findings reveal that increasing curvature promotes the UJT by reducing the energy barriers to cellular rearrangements. Higher curvature favors cell intercalation, mobility, and self-diffusivity, resulting in epithelial structures that are malleable and migratory when small, but become more rigid and stationary as they grow. Together, these results provide a conceptual framework to better understand how cell shape, cell propulsion, and tissue geometry contribute to tissue malleability, remodeling, and stabilization.

DOI: 10.1103/PhysRevLett.134.138402

To heal a wound, remodel tissues, or invade surrounding structures, the confluent epithelial layer transitions from a sedentary, quiescent state to a highly migratory and dynamic one [1,2]. This phenotypic switch has been interpreted as the unjamming transition (UJT) [3–17]. In the jammed phase, cellular rearrangements are rare because cells are locked in place by neighbors, leading to tissue rigidity. In the unjammed phase, cells move cooperatively with neighbors, leading to tissue fluidity and malleability [18–21].

Theoretical models have characterized the UJT in epithelial layers on flat surfaces [22–30]. By contrast, epithelial layers *in vivo* often reside on strongly curved surfaces, where the radius of curvature can be as small as several cell diameters. Examples include spherical pulmonary alveoli, tubular small airways, and ellipsoidal embryos [31–33]. Experiments show that such curved geometries alter epithelial plasticity: topological defects and out-of-plane forces impact cell packing and cytoskeletal organization [31,32,34–41]. Curvature influences migration and cooperativity, inducing coherent rotational motions and cell alignment [34,35,38,39,41].

Previous theoretical models have studied tissue plasticity of curved epithelia in the contexts of the developing neural tube, the fly leg disk, and the mouse optical cup [42–46]. However, these particular geometries make it difficult to isolate the intrinsic effects of surface curvature from those induced by topological constraints. As such, the mechanistic role of surface curvature on cell packing, mobility, and the resulting unjamming dynamics remains poorly understood.

To fill this gap, here we embed a vertex model (VM) [5,15,24,47–49] onto a spherical surface. Using this spherical VM, we investigate the UJT within physiological ranges of cell density and surface curvature. We show that, as surface curvature progressively increases, energy barriers to cellular rearrangements progressively decrease. In the presence of cellular propulsion, increasing curvature favors cell migration, larger self-diffusivity, and more frequent intercalation events.

Our Letter is significant in several ways. First, it suggests that developing curved structures are unjammed, fluidlike, and malleable when small but become more jammed, solidlike, and rigid as they grow. Second, it identifies a novel mechanism of epithelial layer fluidization: curvature-induced unjamming. Finally, it offers a quantitative framework to understand how cell shape, propulsion, and tissue geometry together contribute to the migratory phenotype *in vivo*.

The spherical vertex model—We embed a 3D apical vertex model [23,24,42,43,50,51] onto a spherical topology (Fig. 1). The apical surface of cells is specified by the vertices' locations, constrained to the spherical surface. Cell edges are defined by geodesic curves connecting adjacent vertices. We define the system's mechanical energy as $E = \sum_{i=1}^{N} [K_A(A_i - A_0)^2 + K_P(P_i - P_0)^2]$. A_i and P_i are the apical area and perimeter of the ith cell,

*Contact author: nhmdm@channing.harvard.edu
†Contact author: d.bi@northeastern.edu

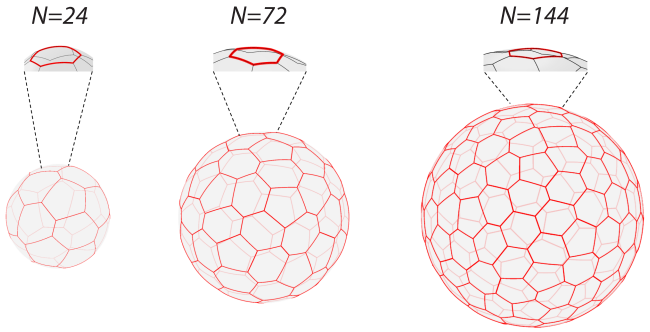

FIG. 1. Spherical VMs with various cell numbers N, corresponding to sphere radii $R = 1.38, 2.39, 3.38$. Spheres with lower N exhibit higher surface curvature.

calculated from the geodesic polygons enclosed by the vertices [23,25,42,51,52]. A_0 and P_0 are the preferred area and perimeter, homogeneous across all N cells. K_A and K_P are the elastic moduli for area and perimeter deformations. This energy function accounts for cell incompressibility [51,53], tissue bulk and actomyosin cortex elasticities [51–54], and the balance between cell-cell adhesion and cortical tension [23,30,51,52]. We set $A_0 = \bar{A}$, with $\bar{A}$ the average cell area. Choosing $K_P\bar{A}$ as the energy unit and $\sqrt{\bar{A}}$ as the length unit, the energy functional reduces to

$$\epsilon = \sum_{i=1}^{N} [k_A(a_i - 1)^2 + (p_i - p_0)^2], \tag{1}$$

where $a_i = A_i/\bar{A}$ and $p_i = P_i/\sqrt{\bar{A}}$ are the rescaled cell area and perimeter. $k_A = K_A\bar{A}/K_P$ is the rescaled area elasticity and $p_0 = P_0/\sqrt{\bar{A}}$ is the dimensionless target shape index.

We examine the spherical VM at various radii of curvature while isolating the influence of number density. We therefore choose $R = \sqrt{N/4\pi}$ such that each cell has mean unit area. Consequently, spherical surfaces with fewer cells N exhibit higher curvature (Fig. 1). Different system sizes $N = 36$–360 are analyzed, corresponding to radii of curvature in the range of 1.69–5.35 times the mean cell size. This constitutes a physiologically relevant range experienced by cells in curved epithelia [41]. A range of p_0 and k_A values is studied at each N. For each parameter choice, we use a combination of the first-order conjugate gradient and second-order Newton's method to find the nearest local energy minima [55,56] (Supplemental Material [57]). For each equilibrium configuration, we perform T1 transitions on each edge to calculate the corresponding energy barrier. Using the same energy minimization scheme, we simulate also a flat VM of $N = 300$ cells. Finally, we examine the spherical VM in the presence of cell motility at various curvatures and fixed $p_0 = 3.65$ (see Ref. [57]). This p_0 value ensures the single-cell dynamics to remain Brownian for all analyzed N values.

Curvature promotes epithelial fluidity—We first study how substrate geometry influences tissue rigidity. In the case of flat surfaces, the vertex model predicts a rigidity transition at the critical value $p_0 = p_0^* \sim 3.81$ [23–25,30,58]. This transition is driven by a percolation transition of the tissue's tension network, defined as the network of edges with tension $\tau > 0$ [30,58,59]. We examine the spatial organization of the tension network in the spherical VM (Supplemental Material [57]).

At fixed curvature, the tension network displays a behavior analogous to the flat surface. At lower p_0 [Fig. 2(a) left panel], the network forms a system-spanning structure and the tissue is completely rigid. By increasing p_0, the network segregates progressively into disconnected components that are reminiscent of a fluidlike phase [30] [central and right panels of Fig. 2(a)]. We quantify this behavior at different curvatures by calculating the probability of tension percolation F_{perc} at various p_0 and N [Fig. 2(b), Supplemental Material [57]]. Similar to the flat tissue, F_{perc} decays with p_0 as an error function. F_{perc} becomes sharper and more heavy tailed by increasing N, as expected due to finite-size effects [30]. Increasing N also shifts F_{perc} toward higher values of p_0, suggesting a role of curvature that goes beyond finite-size scaling. In confirmation of this role, the tension percolation threshold $p_0^*(N)$, and hence the onset of rigidity, decreases by increasing the surface curvature [Fig. 2(c), Supplemental Material [57]]. In the zero-curvature limit $N \to \infty$, $p_0^*(N)$ approaches the flat limit $p_0^*(\infty) \sim 3.814$. F_{perc} collapses onto a single curve after shifting by $p_0^*(N)$ and rescaling by the finite-size scaling law $N^{1/2\nu}$, with $\nu = 0.6$ [inset of Fig. 2(b)]. Notably, the shift in the onset of rigidity can be understood

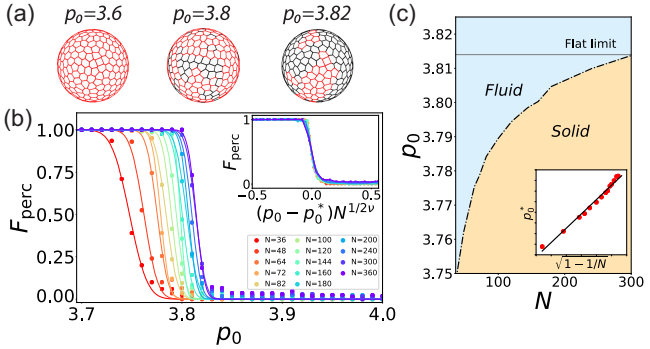

FIG. 2. (a) The tension network at $N = 300$, $k_A = 1$, and various p_0. Red edges have finite tension. (b) Probability of tension percolation F_{perc} versus p_0 for different N at $k_A = 1$. $F_{\mathrm{perc}}(p_0, N)$ is well described by $1/2\{1 - \mathrm{erf}[(p_0 - \mu_N)/(\sqrt{2}\sigma_N)]\}$ (solid lines). When F_{perc} is rescaled by finite-size effects ($N^{1/2\nu}$, $\nu = 0.6$) and shifted by the percolation threshold $p_0^*(N)$, F_{perc} collapses onto a single curve (inset). (c) Phase diagram of the spherical VM. The percolation threshold $p_0^*(N)$ (dashed line), marking the onset of rigidity, increases with N. Inset: in agreement with our predictions, $p_0^* \propto \sqrt{1 - 1/N}$.

within the framework of geometric compatibility. Increasing curvature in our model is analogous to applying isotropic strain: higher curvature uniformly compresses cell perimeters while keeping cell areas fixed. This analogy allows us to derive the dependence of p_0^* on N using recent findings on underconstrained spring networks [60,61] (Supplemental Material [57]). Indeed, we can predict $p_0^*(N)$ to scale as $p_0^*(N) \propto \sqrt{1-1/N}$. Our simulations confirm this prediction, as shown in the inset of Fig. 2(c). These results indicate that curvature promotes tissue fluidization.

Curvature lowers the energy barrier for cellular rearrangements—To gain mechanistic insights on the curvature-induced fluidization, we examine the mechanical response of the tissue to external perturbations. Under confluency, tissue fluidity is driven by cells' ability to rearrange via $T1$ transitions [Fig. 3(a)] [62–68]. We hypothesize that tissue curvature impacts rigidity by affecting the energy ΔU required to execute a $T1$ transition, defined as the energy cost to collapse an edge into a fourfold vertex (Supplemental Material [57]). We test this by studying how ΔU changes with curvature.

At fixed $p_0 = 3.5$ and $k_A = 1$, ΔU decreases on average with increasing curvature [Fig. 3(b)]. This confirms that curvature favors cell intercalations energetically. To understand this behavior, we delve into the underlying mechanism

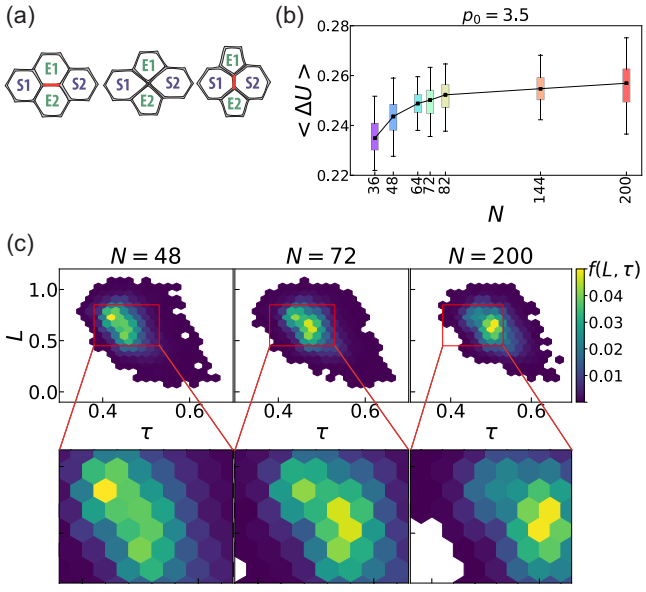

FIG. 3. (a) Schematic of a $T1$ transition. Left: cells $E1$ and $E2$ share initially an edge (orange line). Center: the edge is collapsed into a fourfold vertex. Right: a new edge is created between cells $S1$ and $S2$ (orange line). (b) Whisker plots of ΔU versus N at fixed $p_0 = 3.5$ and $k_A = 1$. Boxes span from the first to the third quartile. Whiskers extend to the farthest data point within 1.5 times the interquartile range from the box. The black line indicates the median. (c) Distributions of edge lengths L and tensions τ (top panels, magnification in bottom panels) at $N = 48$, 72, 200, $p_0 = 3.5$, and $k_A = 1$.

of $T1$ transitions. During a $T1$, tissue energy is impacted by two effects (Supplemental Material [57]): (1) the pure topological rearrangement of the connectivity network and (2) the relaxation of the surrounding vertices to reach a new stable configuration. We study these contributions separately. Interestingly, the relaxation and topological terms are positively correlated as $\Delta U_{\mathrm{rel}} \sim \eta \Delta U_{\mathrm{top}}$, with η being independent of N (Supplemental Material [57]).

The functional dependence of ΔU_{top} can be predicted by developing a simple geometric ansatz. When an edge is collapsed, $\Delta U_{\mathrm{top}} = \Delta U_{\mathrm{per}} + \Delta U_{\mathrm{area}}$ is defined only by the changes in area ΔU_{area} and perimeter ΔU_{per} of the four cells involved in the $T1$. In a mean-field approximation, ΔU_{per} and ΔU_{area} can be derived analytically (see Ref. [57]),

$$\Delta U_{\mathrm{per}} = AL^2 + BL\tau_S + C L\tau; \;\; \Delta U_{\mathrm{area}} = k_A[\sin(2\pi/3)L^2]^2. \tag{2}$$

L and τ represent the initial length and tension of the collapsed edge. $\tau_S = p_{S1} + p_{S2} - 2p_0$ expresses the deviation of the rescaled perimeters of cells S_1 and S_2 [Fig. 3(a)] from p_0. A, B, and C are numerical factors with values $A = 1.085$, $B = 1.29$, $C = -0.708$. As such, ΔU_{per} depends only on the local properties of (1) the collapsed edge before the $T1$ and (2) the surrounding cells S_1 and S_2. Similar to previous reports [23,24,69], Eq. (2) includes a quadratic dependence of ΔU_{per} on L. Our model reveals also a linear dependence on the edge tension that is modulated by L. Hence, $T1$ transitions are energetically penalized on both longer and more tense edges.

By combining the relationship between ΔU_{rel} and ΔU_{top} with Eq. (2), we recapitulate the behavior of ΔU. ΔU shows no significant changes between edge configurations with same (L, τ, τ_S) values but different N (Supplemental Material [57]). At fixed (τ, τ_S, p_0), ΔU collapses onto a single master curve that is independent of curvature and is well described by our mean-field model (see Ref. [57]). Such collapse occurs regardless of the p_0 value. Our predictions hold also on flat surfaces (see Ref. [57]), confirming the universality of Eq. (2).

Our findings show that the $T1$'s energetic cost depends solely on the local properties of the edge network. Surface curvature does not impact the $T1$'s dependence on these properties. This suggests that the curvature-induced fluidization does not stem from local changes in the individual $T1$ mechanism, but rather from global changes in the edge network.

In the absence of cell motility, curvature of the jammed layer impacts the distributions of edge lengths and edge tensions—To understand how changes in the cell-junctional network impact tissue rigidity, we first investigate the density distribution of edge length and tensions, $f(L, \tau)$, at $p_0 = 3.5, k_A = 1$. Figure 3(c) confirms that curvature significantly alters $f(L, \tau)$. Consistent with our percolation analysis, the tension distribution $f(\tau)$ shifts toward larger τ

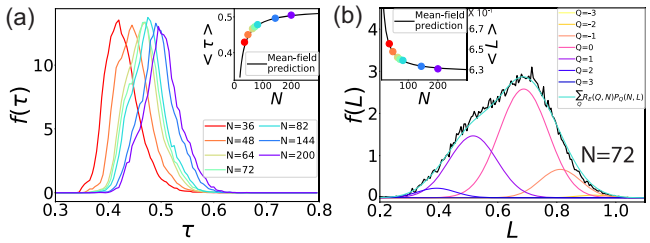

FIG. 4. (a) Density distribution $f(\tau)$ of edge tensions for spheres with different N at $p_0 = 3.5, k_A = 1$. Inset: average edge tension $\langle\tau\rangle$ versus N. The solid line corresponds to Eq. (4), with $P_{\text{flat}} = 3.76$ equal to the average perimeter at the largest $N = 360$. (b) Density distribution $f(L)$ of edge lengths at $N = 72, p_0 = 3.5, k_A = 1$ (black line). Colored solid lines correspond to Gaussian fits of the densities $f_Q(L)$. The turquoise line corresponds to the weighted sum of the Gaussian fits $\sum_Q R_E(Q) f_Q(L)$, where $R_E(Q)$ is the fraction of edges with given Q over the total. Inset: average edge length $\langle L\rangle$ versus N at $p_0 = 3.5$ and $k_A = 1$. The solid line corresponds to Eq. (3), with $P_{\text{flat}} = 3.76$ equal to the average perimeter at the largest $N = 360$.

values at higher N [Fig. 4(a)]. The distribution of edge lengths $f(L)$ exhibits a more intriguing behavior. On flat surfaces, $f(L)$ has been traditionally reported as a Gaussian [24]. On the spherical layer, however, $f(L)$ appears as the sum of multiple Gaussians $e^{(x-\mu)/\sigma}$ [Fig. 4(b)]. These Gaussians coincide with distinct contact topologies around the edge. Indeed, we find (μ, σ) to be parametric in the quantity $Q = 6 - Z_{S1} + 6 - Z_{S2}$, where Z_{S1} and Z_{S2} are the number of neighbors of cells $S1$ and $S2$ [24] [Fig. 3(a)]. Edges are shorter at higher values of Q, corresponding to $S1, S2$ pairs with fewer neighbors. We observe similar behavior on flat surfaces (Supplemental Material [57]), where a monotonic decrease of ΔU with Q has been reported [24]. Our results offer mechanistic insights: shorter cell edges at larger Q reduce the energetic cost of cellular rearrangements.

We analyze the edge length distribution $f_Q(L)$ at different Q and radii of curvature. The average length μ_Q decreases with N for each Q, while the ratio of edges with given Q varies nonmonotonically with N (Supplemental Material [57]). This leads to an average increase of L with increasing curvature [inset of Fig. 4(b)].

The dependence of edge lengths and tensions on N can be explained through geometric arguments. The perimeter P of a spherical polygon is related to its equivalent P_{flat} on the flat surface via the identity $P(N) = P_{\text{flat}}\sqrt{1 - 1/N}$ (Supplemental Material [57] and Ref. [70]). By combining this scaling with Euler's polyhedron formula, we can derive the average length $\langle L\rangle$ and tension $\langle\tau\rangle$,

$$\langle L\rangle \approx \langle P\rangle/\langle Z\rangle \approx \frac{\langle P_{\text{flat}}\rangle\sqrt{1 - 1/N}}{6 - 12/N}; \tag{3}$$

$$\langle\tau\rangle \approx 2\langle P\rangle - 2P_0 = \tau_{\text{flat}} + A_\tau\left(-1 + \sqrt{1 - 1/N}\right), \tag{4}$$

where $\tau_{\text{flat}} = 2\langle P_{\text{flat}}\rangle - 2P_0$ and $A_\tau = 2\langle P_{\text{flat}}\rangle$. $\langle\rangle$ denotes the average over all equilibrium configurations with given (N, p_0, k_A) obtained via our energy minimization scheme. Both Eqs. (3) and (4) recapitulate our simulation results [insets of Figs. 4(a) and 4(b) and Supplemental Material [57]]. As such, curvature impacts the cell network's spatial (edge lengths) and mechanical (edge tensions) configuration in opposite ways. These effects, in turn, impact tissue rigidity in opposite ways: longer edges penalize cell rearrangements, while lower intercellular tensions favor cell intercalation. Notably, Eq. (4) provides information also on the density distribution $f(\tau_S)$. $f(\tau_S)$ exhibits the same trend as $f(\tau)$ when varying N (Supplemental Material [57]). Since τ and τ_S are theoretically equivalent on average, Eq. (4) correctly predicts the dependence of $\langle\tau_S\rangle$ on curvature (see Ref. [57]).

Equation (3) implies that the edge length distribution arises from the interplay of two constraints: the spherical constraint, which forces cells with the same area and higher curvature to have smaller perimeters, and the topological constraint, which forces the average number of cell neighbors to decrease with curvature. This latter effect dominates the behavior of $\langle L\rangle$, but is insufficient to explain alone its overall dependency on N. To test this, we compare our spherical VM with a spherical Voronoi tessellation, where varying N changes only the number of topological defects (defined as deviations from a regular hexagonal cellular network) but not the surface curvature. Our simulations confirm that the decrease of $\langle L\rangle$ with N due to the topological constraints of the Voronoi sphere does not recapitulate the behavior shown in Fig. 4(b) (Supplemental Material [57]).

The results presented so far have been derived at fixed area elasticity $k_A = 1$. Given that the edge network at equilibrium depends on k_A, in principle, we ask whether different k_A values affect the curvature-induced rigidity transition. Based on our mean-field model, we expect $f(L)$ and $f(\tau)$, and hence p_0^*, to be independent of k_A (Supplemental Material [57]). Analysis of the spherical VM at various k_A confirms that, to the leading order, the impact of the area elasticity on the rigidity transition is negligible (see Ref. [57]).

Cell packing also affects the edge network's configuration. Thus, we explore how the cell density ρ impacts the rigidity of our spherical VM by relaxing the uniform density constraint $R = \sqrt{N/4\pi}$. Analogous to the flat VM, increasing ρ decreases the overall edge tension, shifting the onset of rigidity to lower p_0. For $\rho < 1$, the average edge tension collapses onto a single curve after rescaling p_0 by the average cell area. This suggests that the density-dependent changes in the cell tension network are trivially due to the corresponding changes in cell areas.

Conversely, for $\rho > 1$, tissue rigidity is affected by additional nontrivial factors beyond the changes in cell area (Supplemental Material [57]).

In the presence of cell motility, curvature promotes cellular migration—We further investigate how curvature affects tissue fluidity in the presence of cell motility. We consider the interplay between cell motility and substrate frictional drag [41]. In this description, the change rate of position $\vec{r}_i$ of the ith vertex obeys the overdamped equation of motion $\Gamma d\vec{r}_i/dt = \vec{F}_i^{\text{int}} + v_0\hat{n}_i$, where Γ is the frictional damping coefficient. $\vec{F}_i^{\text{int}}$ summarizes intercellular interactions mediated by cell-cell contacts and $v_0\hat{n}_i$ represents cellular tractions applied on the substrate. Cell polarization vectors $\hat{n}_i$ undergo rotational diffusion with rate D_r [71–73] (Supplemental Material [57]).

We first analyze the cell dynamics of the spherical layer at fixed $v_0 = 0.09$, $p_0 = 3.65$, and $k_A = 1$. This choice of parameters ensures that the single-cell dynamics remains Brownian across all the investigated radii of curvature. The average cell mean-square displacement $\langle \Delta r^2(t) \rangle$ displays three temporal regimes that are reminiscent of glassy dynamics [Fig. 5(a)]: an early-time ballistic regime, an intermediate switching regime that resembles a plateau, and a long-time diffusive regime. For each N, we calculate the self-diffusion coefficient D_{eff} in units of the free diffusion constant D_0 of an isolated cell. D_{eff} is defined as $D_{\text{eff}} = D_s/D_0$, where $D_s = \lim_{t\to\infty} \langle \Delta r^2(t) \rangle/(4t)$ and $D_0 = v_0^2/(2D_r)$. D_{eff} shows a strong dependence on curvature, exhibiting higher values at lower N (Supplemental Material [57]). Similarly, the cumulative number N_{T1} of $T1$ transitions per junction over time decreases with N [Fig. 5(a) inset].

We further measure D_{eff} and the rate of $T1$ transitions k_{T1} for several combinations of v_0 and N. At fixed N, there is a motility-driven solid-fluid transformation [Fig. 5(b)]. Notably, surface curvature modulates the cell motility threshold v_0^* at which this transition occurs. v_0^* increases nonmonotonically with N, reaching an asymptotic plateau for $N > 75$ where the effect of curvature becomes negligible [Fig. 5(b)]. Hence, all other factors being equal, the epithelial layer is more fluidlike and unjammed when it resides upon more curved surfaces.

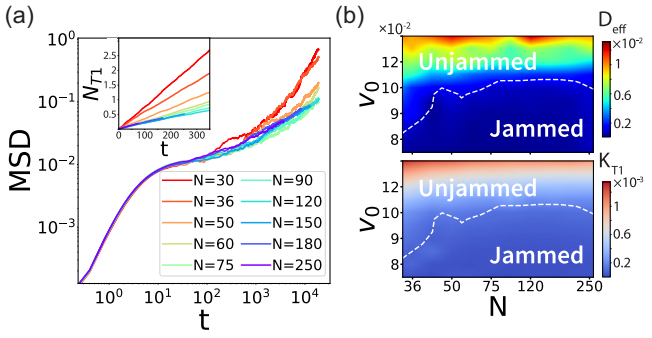

FIG. 5. (a) Mean-square displacement (MSD) on sphere varying N at $p_0 = 3.65, k_A = 1, v_0 = 0.09$. Inset: cumulative count of $T1$ per junction versus time. (b) Heat maps of the diffusion coefficient D_{eff} (upper) and $T1$ rate k_{T1} (lower) as a function of N and v_0 at fixed $p_0 = 3.65$ and $k_A = 1$. The dashed line represents the motility-driven transition $v_0^*(N)$, where $D_{\text{eff}} = 0.001$ [25,74].

Discussion—Our model indicates that increasing curvature induces fluidization and migration. This is not due to changes in the local mechanism of cell intercalation, which is independent of curvature, but rather to changes in the global structure of the cell-junction network, which becomes less tensed with increased curvature. Cell rearrangements become energetically advantageous at higher curvatures, resulting in cellular configurations that are more malleable and more migratory.

Part of our results is supported by recent works on the spherical VM [75–77]. Different from these studies, however, our Letter is the first to (1) investigate the effect of curvature on both tissue's mechanical stability and migratory behavior and (2) identify its underlying mechanism. In doing so, we offer testable hypotheses about how tissue mechanics respond to substrate curvature. Recent experiments on lung alveolospheres showed that curvature enhances fluidity by modifying the cell packing distribution [41]. Our Letter demonstrates that curvature affects the cell rearrangements rate by altering the cell-cell contact network, providing a mechanistic framework for understanding these experimental results. Our results also suggest that measuring junctional tensions (e.g., via localized laser ablation [78] or laser tweezers [79]) can serve as a direct indicator of tissue rigidity on curved surfaces. This new predictive metric could be employed to distinguish between different mechanical phases in organoid models.

Our findings stem from the isotropic nature of the spherical VM and its constant cell density. This geometry is ideal for understanding the intrinsic effects of surface curvature and is relevant to various physiological and pathological contexts [35,41,80,81]. Anisotropic curved geometries may show more complex behaviors, with nontrivial dependencies on area elasticity or asymmetries in cell tension. Our Letter lays the groundwork for future studies on these geometries, such as tubes, ellipsoids, and toroids. Further analysis is also necessary to elucidate the role of cell packing density on the rigidity of curved epithelia. Similarly, further research is needed to understand how our findings translate to a 3D model of curved epithelia [82,83]. For surface patches with varying principal curvatures, such as those observed in epithelial monolayers on wavy patterns [84], mechanical contributions from the basal and lateral surfaces create heterogeneous stress distributions. This can affect cell packing, motility, and unjamming transitions. Regions with higher curvature may fluidize more easily due to lower energy costs for cell rearrangements, while flatter regions may remain rigid. Future work should develop a 3D vertex model [82,85] to provide insights into the full mechanics of curved epithelia, considering the apical, basal, and lateral surfaces.

Acknowledgments—The authors acknowledge the support of the Northeastern University Discovery Cluster. M. D. M. acknowledges support from the National Heart Lung and Blood Institute (Grant No. NHLBI K25HL168157). A. D. acknowledges support from the New Faculty SEED Grant from IIT Delhi, India and the Start-up Research Grant from SERB-DST, Government of India (Grant No. SRG/2023/000099). D. B. acknowledges support from the National Science Foundation (Grant No. DMR-2046683 and No. PHY-2019745), the NIGMS of the National Institutes of Health (NIH) (Grant No. R35GM15049), the Alfred P. Sloan Foundation, and the Human Frontier Science Program (Ref. No. RGP0007/2022). J. J. F. acknowledges support from the National Heart Lung and Blood Institute (Grant No. NHLBI 1R01HL148152 and No. T32HL007118).

[1] Peter Friedl and Darren Gilmour, Collective cell migration in morphogenesis, regeneration and cancer, Nat. Rev. Mol. Cell Biol. **10**, 445 (2009).
[2] Pernille Rorth, Collective cell migration, Annu. Rev. Cell Dev. Biol. **25**, 407 (2009).
[3] Lior Atia, Dapeng Bi, Yasha Sharma, Jennifer A. Mitchel, Bomi Gweon, Stephan A. Koehler, Stephen J. DeCamp, Bo Lan, Jae Hun Kim, Rebecca Hirsch *et al.*, Geometric constraints during epithelial jamming, Nat. Phys. **14**, 613 (2018).
[4] Jin-Ah Park, Lior Atia, Jennifer A. Mitchel, Jeffrey J. Fredberg, and James P. Butler, Collective migration and cell jamming in asthma, cancer and development, J. Cell Sci. **129**, 3375 (2016).
[5] Jin-Ah Park, Jae Hun Kim, Dapeng Bi, Jennifer A. Mitchel, Nader Taheri Qazvini, Kelan Tantisira, Chan Young Park, Maureen McGill, Sae-Hoon Kim, Bomi Gweon *et al.*, Unjamming and cell shape in the asthmatic airway epithelium, Nat. Mater. **14**, 1040 (2015).
[6] Jennifer A. Mitchel, Amit Das, Michael J. O'Sullivan, Ian T. Stancil, Stephen J. DeCamp, Stephan Koehler, Oscar H. Ocaña, James P. Butler, Jeffrey J. Fredberg, M. Angela Nieto *et al.*, In primary airway epithelial cells, the unjamming transition is distinct from the epithelial-to-mesenchymal transition, Nat. Commun. **11**, 5053 (2020).
[7] Lior Atia, Jeffrey J. Fredberg, Nir S. Gov, and Adrian F. Pegoraro, Are cell jamming and unjamming essential in tissue development?, Cells Dev. **168**, 203727 (2021).
[8] Linda Oswald, Steffen Grosser, David M. Smith, and Josef A. Käs, Jamming transitions in cancer, J. Phys. D **50**, 483001 (2017).
[9] Jin-Ah Park and Jeffrey J. Fredberg, Cell jamming in the airway epithelium, Ann. Am. Thorac. Soc. **13**, S64 (2016).
[10] Adrian F. Pegoraro, Jeffrey J. Fredberg, and Jin-Ah Park, Problems in biology with many scales of length: Cell–cell adhesion and cell jamming in collective cellular migration, Exp. Cell Res. **343**, 54 (2016).
[11] Monirosadat Sadati, Nader Taheri Qazvini, Ramaswamy Krishnan, Chan Young Park, and Jeffrey J. Fredberg, Collective migration and cell jamming, Differentiation (Berlin) **86**, 121 (2013).
[12] Margherita De Marzio, Ayşe Kılıç, Enrico Maiorino, Jennifer A. Mitchel, Chimwemwe Mwase, Michael J. O'Sullivan, Maureen McGill, Robert Chase, Jeffrey J. Fredberg, Jin-Ah Park *et al.*, Genomic signatures of the unjamming transition in compressed human bronchial epithelial cells, Sci. Adv. **7**, eabf1088 (2021).
[13] Junxiang Huang, James O. Cochran, Suzanne M. Fielding, M. Cristina Marchetti, and Dapeng Bi, Shear-driven solidification and nonlinear elasticity in epithelial tissues, Phys. Rev. Lett. **128**, 178001 (2022).
[14] Haiqian Yang, Adrian F. Pegoraro, Yulong Han, Wenhui Tang, Rohan Abeyaratne, Dapeng Bi, and Ming Guo, Configurational fingerprints of multicellular living systems, Proc. Natl. Acad. Sci. U.S.A. **118**, e2109168118 (2021).
[15] Michael J. Hertaeg, Suzanne M. Fielding, and Dapeng Bi, Discontinuous shear thickening in biological tissue rheology, Phys. Rev. X **14**, 011027 (2024).
[16] Grace Cai, Anh Nguyen, Yashar Bashirzadeh, Shan-Shan Lin, Dapeng Bi, and Allen P. Liu, Compressive stress drives adhesion-dependent unjamming transitions in breast cancer cell migration, Front. Cell Dev. Biol. **10**, 933042 (2022).
[17] Grace Cai, Xinzhi Li, Shan-Shan Lin, Samuel J. Chen, Nicole C. Rodgers, Katherine M. Koning, Dapeng Bi, and Allen P. Liu, Matrix confinement modulates 3d spheroid sorting and burst-like collective migration, Acta Biomater. **179**, 192 (2024).
[18] Thomas E. Angelini, Edouard Hannezo, Xavier Trepat, Manuel Marquez, Jeffrey J. Fredberg, and David A. Weitz, Glass-like dynamics of collective cell migration, Proc. Natl. Acad. Sci. U.S.A. **108**, 4714 (2011).
[19] Kenechukwu David Nnetu, Melanie Knorr, Steve Pawlizak, Thomas Fuhs, and Josef A. Käs, Slow and anomalous dynamics of an mcf-10a epithelial cell monolayer, Soft Matter **9**, 9335 (2013).
[20] Shao-Zhen Lin, Wu-Yang Zhang, Dapeng Bi, Bo Li, and Xi-Qiao Feng, Energetics of mesoscale cell turbulence in two-dimensional monolayers, Commun. Phys. **4**, 21 (2021).
[21] Juan P. Garrahan, Dynamic heterogeneity comes to life, Proc. Natl. Acad. Sci. U.S.A. **108**, 4701 (2011).
[22] Ricard Alert and Xavier Trepat, Physical models of collective cell migration, Annu. Rev. Condens. Matter Phys. **11**, 77 (2020).
[23] Dapeng Bi, J. H. Lopez, Jennifer M. Schwarz, and M. Lisa Manning, A density-independent rigidity transition in biological tissues, Nat. Phys. **11**, 1074 (2015).
[24] Dapeng Bi, Jorge H. Lopez, Jennifer M. Schwarz, and M. Lisa Manning, Energy barriers and cell migration in densely packed tissues, Soft Matter **10**, 1885 (2014).
[25] D. Bi, X. Yang, M. C. Marchetti, and M. L. Manning, Motility-driven glass and jamming transitions in biological tissues, Phys. Rev. X **6**, 021011 (2016).
[26] T. Vicsek, A. Czirók, E. Ben-Jacob, I. Cohen, and O. Shochet, Novel type of phase transition in a system of self-driven particles, Phys. Rev. Lett. **75**, 1226 (1995).
[27] Silke Henkes, Yaouen Fily, and M. Cristina Marchetti, Active jamming: Self-propelled soft particles at high density, Phys. Rev. E **84**, 040301(R) (2011).
[28] M. Chiang and D. Marenduzzo, Glass transitions in the cellular potts model, Europhys. Lett. **116**, 28009 (2016).

[29] Michael Czajkowski, Daniel M. Sussman, M. Cristina Marchetti, and M. Lisa Manning, Glassy dynamics in models of confluent tissue with mitosis and apoptosis, Soft Matter **15**, 9133 (2019).
[30] Xinzhi Li, Amit Das, and Dapeng Bi, Mechanical heterogeneity in tissues promotes rigidity and controls cellular invasion, Phys. Rev. Lett. **123**, 058101 (2019).
[31] Hannah G. Yevick, Guillaume Duclos, Isabelle Bonnet, and Pascal Silberzan, Architecture and migration of an epithelium on a cylindrical wire, Proc. Natl. Acad. Sci. U.S.A. **112**, 5944 (2015).
[32] Tianchi Chen, Andrew Callan-Jones, Eduard Fedorov, Andrea Ravasio, Agustí Brugués, Hui Ting Ong, Yusuke Toyama, Boon Chuan Low, Xavier Trepat, Tom Shemesh *et al.*, Large-scale curvature sensing by directional actin flow drives cellular migration mode switching, Nat. Phys. **15**, 393 (2019).
[33] Maxime Vassaux, Laurent Pieuchot, Karine Anselme, Maxence Bigerelle, and Jean-Louis Milan, A biophysical model for curvature-guided cell migration, Biophys. J. **117**, 1136 (2019).
[34] Alexandros Glentis, Carles Blanch-Mercader, Lakshmi Balasubramaniam, Thuan Beng Saw, Joseph d'Alessandro, Sebastien Janel, Audrey Douanier, Benedicte Delaval, Frank Lafont, Chwee Teck Lim *et al.*, The emergence of spontaneous coordinated epithelial rotation on cylindrical curved surfaces, Sci. Adv. **8**, eabn5406 (2022).
[35] Tom Brandstätter, David B. Brückner, Yu Long Han, Ricard Alert, Ming Guo, and Chase P. Broedersz, Curvature induces active velocity waves in rotating spherical tissues, Nat. Commun. **14**, 1643 (2023).
[36] Maike Werner, Nicholas A. Kurniawan, Gabriela Korus, Carlijn V. C. Bouten, and Ansgar Petersen, Mesoscale substrate curvature overrules nanoscale contact guidance to direct bone marrow stromal cell migration, J. R. Soc. Interface **15**, 20180162 (2018).
[37] Pablo Rougerie, Laurent Pieuchot, Rafaela Silva Dos Santos, Julie Marteau, Maxence Bigerelle, Pierre-François Chauvy, Marcos Farina, and Karine Anselme, Topographical curvature is sufficient to control epithelium elongation, Sci. Rep. **10**, 14784 (2020).
[38] Wang Xi, Surabhi Sonam, Thuan Beng Saw, Benoit Ladoux, and Chwee Teck Lim, Emergent patterns of collective cell migration under tubular confinement, Nat. Commun. **8**, 1517 (2017).
[39] Caterina Tomba, Valeriy Luchnikov, Luca Barberi, Carles Blanch-Mercader, and Aurélien Roux, Epithelial cells adapt to curvature induction via transient active osmotic swelling, Dev. Cell **57**, 1257 (2022).
[40] H. G. Yevick, G. Duclos, I. Bonnet, and P. Silberzan, Architecture and migration of an epithelium on a cylindrical wire, Proc. Natl. Acad. Sci. U.S.A. **112**, 5944 (2015).
[41] Wenhui Tang, Amit Das, Adrian F. Pegoraro, Yu Long Han, Jessie Huang, David A. Roberts, Haiqian Yang, Jeffrey J. Fredberg, Darrell N. Kotton, Dapeng Bi *et al.*, Collective curvature sensing and fluidity in three-dimensional multicellular systems, Nat. Phys. **18**, 1371 (2022).
[42] Alexander G. Fletcher, Miriam Osterfield, Ruth E. Baker, and Stanislav Y. Shvartsman, Vertex models of epithelial morphogenesis, Biophys. J. **106**, 2291 (2014).
[43] Silvanus Alt, Poulami Ganguly, and Guillaume Salbreux, Vertex models: From cell mechanics to tissue morphogenesis, Phil. Trans. R. Soc. B **372**, 20150520 (2017).
[44] Bruno Monier, Melanie Gettings, Guillaume Gay, Thomas Mangeat, Sonia Schott, Ana Guarner, and Magali Suzanne, Apico-basal forces exerted by apoptotic cells drive epithelium folding, Nature (London) **518**, 245 (2015).
[45] Yasuhiro Inoue, Makoto Suzuki, Tadashi Watanabe, Naoko Yasue, Itsuki Tateo, Taiji Adachi, and Naoto Ueno, Mechanical roles of apical constriction, cell elongation, and cell migration during neural tube formation in xenopus, Biomech. Model. Mechanobiol. **15**, 1733 (2016).
[46] Mototsugu Eiraku, Nozomu Takata, Hiroki Ishibashi, Masako Kawada, Eriko Sakakura, Satoru Okuda, Kiyotoshi Sekiguchi, Taiji Adachi, and Yoshiki Sasai, Self-organizing optic-cup morphogenesis in three-dimensional culture, Nature (London) **472**, 51 (2011).
[47] Daniel L. Barton, Silke Henkes, Cornelis J. Weijer, and Rastko Sknepnek, Active vertex model for cell-resolution description of epithelial tissue mechanics, PLoS Comput. Biol. **13**, 1 (2017).
[48] Amit Das, Srikanth Sastry, and Dapeng Bi, Controlled neighbor exchanges drive glassy behavior, intermittency, and cell streaming in epithelial tissues, Phys. Rev. X **11**, 041037 (2021).
[49] Xinzhi Li and Dapeng Bi, Nature-inspired designs for disordered acoustic bandgap materials, Soft Matter **19**, 8221 (2023).
[50] Tatsuzo Nagai and Hisao Honda, A dynamic cell model for the formation of epithelial tissues, Philos. Mag. B **81**, 699 (2001).
[51] Reza Farhadifar, Jens-Christian Röper, Benoit Aigouy, Suzanne Eaton, and Frank Jülicher, The influence of cell mechanics, cell-cell interactions, and proliferation on epithelial packing, Curr. Biol. **17**, 2095 (2007).
[52] Douglas B. Staple, Reza Farhadifar, J-C Röper, Benoit Aigouy, Suzanne Eaton, and Frank Jülicher, Mechanics and remodelling of cell packings in epithelia, Eur. Phys. J. E **33**, 117 (2010).
[53] Lars Hufnagel, Aurelio A. Teleman, Hervé Rouault, Stephen M. Cohen, and Boris I. Shraiman, On the mechanism of wing size determination in fly development, Proc. Natl. Acad. Sci. U.S.A. **104**, 3835 (2007).
[54] Steven M. Zehnder, Melanie Suaris, Madisonclaire M. Bellaire, and Thomas E. Angelini, Cell volume fluctuations in MDCK monolayers, Biophys. J. **108**, 247 (2015).
[55] Kenneth A. Brakke, The surface evolver, Exp. Math. **1**, 141 (1992).
[56] Carl T. Kelley, *Iterative Methods for Qptimization* (Society for Industrial and Applied Mathematics, Philadelphia, PA, 1999).
[57] See Supplemental Material at http://link.aps.org/supplemental/10.1103/PhysRevLett.134.138402, which includes additional calculations, methods, supplemental figures.
[58] Le Yan and Dapeng Bi, Multicellular rosettes drive fluid-solid transition in epithelial tissues, Phys. Rev. X **9**, 011029 (2019).
[59] Nicoletta I. Petridou, Bernat Corominas-Murtra, Carl-Philipp Heisenberg, and Edouard Hannezo, Rigidity

percolation uncovers a structural basis for embryonic tissue phase transitions, Cell **184**, 1914 (2021).
[60] Cheng-Tai Lee and Matthias Merkel, Stiffening of underconstrained spring networks under isotropic strain, Soft Matter **18**, 5410 (2022).
[61] Matthias Merkel, Karsten Baumgarten, Brian P. Tighe, and M. Lisa Manning, A minimal-length approach unifies rigidity in underconstrained materials, Proc. Natl. Acad. Sci. U.S.A. **116**, 6560 (2019).
[62] Lara Carvalho, Pedro Patricio, Susana Ponte, Carl-Philipp Heisenberg, Luis Almeida, André S. Nunes, Nuno A. M. Araújo, and Antonio Jacinto, Occluding junctions as novel regulators of tissue mechanics during wound repair, J. Cell Biol. **217**, 4267 (2018).
[63] Elise Walck-Shannon and Jeff Hardin, Cell intercalation from top to bottom, Nat. Rev. Mol. Cell Biol. **15**, 34 (2014).
[64] Kenneth D. Irvine and Eric Wieschaus, Cell intercalation during drosophila germband extension and its regulation by pair-rule segmentation genes, Development **120**, 827 (1994).
[65] Robert J. Tetley, Michael F. Staddon, Davide Heller, Andreas Hoppe, Shiladitya Banerjee, and Yanlan Mao, Tissue fluidity promotes epithelial wound healing, Nat. Phys. **15**, 1195 (2019).
[66] Masazumi Tada and Carl-Philipp Heisenberg, Convergent extension: using collective cell migration and cell intercalation to shape embryos, Development **139**, 3897 (2012).
[67] Matteo Rauzi, Cell intercalation in a simple epithelium, Phil. Trans. R. Soc. B **375**, 20190552 (2020).
[68] Meryl A. Spencer, Zahera Jabeen, and David K. Lubensky, Vertex stability and topological transitions in vertex models of foams and epithelia, Eur. Phys. J. E **40**, 2 (2017).
[69] Preeti Sahu, Janice Kang, Gonca Erdemci-Tandogan, and M. Lisa Manning, Linear and nonlinear mechanical responses can be quite different in models for biological tissues, Soft Matter **16**, 1850 (2020).
[70] Arthur Hernandez, Michael F. Staddon, Michael Moshe, and M. Cristina Marchetti, Finite elasticity of the vertex model and its role in rigidity of curved cellular tissues, Soft Matter **19**, 7744 (2023).
[71] András Szabó, R. Ünnep, Eld Méhes, W. O. Twal, W. S. Argraves, Y. Cao, and András Czirók, Collective cell motion in endothelial monolayers, Phys. Biol. **7**, 046007 (2010).
[72] Benoit Ladoux, René-Marc Mège, and Xavier Trepat, Front–rear polarization by mechanical cues: From single cells to tissues, Trends Cell Biol. **26**, 420 (2016).
[73] Rastko Sknepnek and Silke Henkes, Active swarms on a sphere, Phys. Rev. E **91**, 022306 (2015).
[74] Preeti Sahu, Daniel M. Sussman, Matthias Rübsam, Aaron F. Mertz, Valerie Horsley, Eric R. Dufresne, Carien M. Niessen, M. Cristina Marchetti, M. Lisa Manning, and Jen M. Schwarz, Small-scale demixing in confluent biological tissues, Soft Matter **16**, 3325 (2020).
[75] Daniel M. Sussman, Interplay of curvature and rigidity in shape-based models of confluent tissue, Phys. Rev. Res. **2**, 023417 (2020).
[76] Evan C. Thomas and Sevan Hopyan, Shape-driven confluent rigidity transition in curved biological tissues, Biophys. J. **122**, 4264 (2023).
[77] Aboutaleb Amiri, Charlie Duclut, Frank Jülicher, and Marko Popović, Random traction yielding transition in epithelial tissues, Phys. Rev. Lett. **131**, 188401 (2023).
[78] Rodrigo Fernandez-Gonzalez, Sérgio de Matos Simoes, Jens-Christian Röper, Suzanne Eaton, and Jennifer A. Zallen, Myosin ii dynamics are regulated by tension in intercalating cells, Dev. Cell **17**, 736 (2009).
[79] Kapil Bambardekar, Raphaël Clément, Olivier Blanc, Claire Chardès, and Pierre-François Lenne, Direct laser manipulation reveals the mechanics of cell contacts *in vivo*, Proc. Natl. Acad. Sci. U.S.A. **112**, 1416 (2015).
[80] Anastasiya Trushko, Ilaria Di Meglio, Aziza Merzouki, Carles Blanch-Mercader, Shada Abuhattum, Jochen Guck, Kevin Alessandri, Pierre Nassoy, Karsten Kruse, Bastien Chopard *et al.*, Buckling of an epithelium growing under spherical confinement, Dev. Cell **54**, 655 (2020).
[81] Daria S. Roshal, Karim Azzag, Emilie Le Goff, Sergei B. Rochal, and Stephen Baghdiguian, Crystal-like order and defects in metazoan epithelia with spherical geometry, Sci. Rep. **10**, 7652 (2020).
[82] Jan Rozman, Matej Krajnc, and Primož Ziherl, Collective cell mechanics of epithelial shells with organoid-like morphologies, Nat. Commun. **11**, 3805 (2020).
[83] Yuting Lou, Jean-Francois Rupprecht, Sophie Theis, Tetsuya Hiraiwa, and Timothy E. Saunders, Curvature-induced cell rearrangements in biological tissues, Phys. Rev. Lett. **130**, 108401 (2023).
[84] Marine Luciano, Shi-Lei Xue, Winnok H. De Vos, Lorena Redondo-Morata, Mathieu Surin, Frank Lafont, Edouard Hannezo, and Sylvain Gabriele, Cell monolayers sense curvature by exploiting active mechanics and nuclear mechanoadaptation, Nat. Phys. **17**, 1382 (2021).
[85] Yuting Lou, Jean Francois Rupprecht, Tetsuya Hiraiwa, and Timothy E. Saunders, Curvature-induced cell rearrangements in biological tissues, Phys. Rev. Lett. **130**, 108401 (2023).